Electronic Supplementary Material for "Evidence for convergent evolution of ultrasonic hearing in toothed whales (Cetacea: Odontoceti)"

Authors: Rachel A. Racicot, Robert W. Boessenecker, Simon A.F. Darroch, Jonathan H. Geisler

S1 – Origin of echolocation in Odontocetes

All extant cetaceans lack external ears, and in odontocetes, the sound reaches the inner ear through a large fat pad that extends from the lower jaw to the tympanic bone (Cranford et al. 2008, Cranford et al. 2010, Numella et al. 2007). A large mandibular foramen for housing the fat pads occurs in most archaeocetes, indicating that this sound pathway predates odontocetes and was likely lost in the Mysticeti (baleen whales), the other extant clade of cetaceans (Gatesy et al. 2013, Numella et al. 2007). The middle and inner ear of odontocetes, the receiver component in the sonar analogy, shows several specializations for perceiving ultrasonic (> 20 kHz) sound. The middle ear ossicles are pachyostotic, with the malleus fused to the ectotympanic bulla (Numella et al. 2007). The cochlea has a pronounced secondary bony lamina that extends along at least half of its length, and the basilar membrane is exceptionally thick near its base (Ketten 1992). The morphological specializations are mirrored by molecular changes; the prestin gene is involved in the motility of the hair cells in the organ of Corti, and several mutations that distinguish odontocetes from mysticetes have been shown to increase sensitivity of these cells (Liu et al., 2014). The key sound–producing organ is a pair of phonic lips and associated dorsal bursae (abbreviated as MLDB due to original terminology of "monkey lips" for "phonic lips"); constrictions in the distal soft tissue nasal passages with small fat bodies embedded in the anterior and posterior walls (Cranford et al. 1996; Berta et al. 2014). As air is forced past these constrictions, a dolphin is able to produce a diverse repertoire of sound, with frequencies spanning tens of kilohertz to ultrasonic ranges reaching 170 kHz (Mooney et al. 2012, Galatius et al. 2018). Several other unusual structures are shared by all extant species, including a large fat body, the melon, which transmits and focuses sound produced by the MLDB (McKenna et al. 2012). All odontocetes have air sacs that branch off the distal nasal passages that facilitate the recycling of air for continuous phonation (Reidenberg and Laitman 2008). All of this anatomy is controlled by several muscle groups; facial muscles that have been co-opted to change the shape of the melon and the volume of the air sacs (e.g., Huggenburger et al. 2009, Mead 1975), and

muscles that drive the larynx dorsally into the nasopharyx (e.g., Riedenberg and Laitman 1987, Huggenburger et al. 2008), causing the pressure needed to push air past the MLDB complex.

S2 – Osteological correlates for echolocation on odontocete facial bones

The MLDB complex is entirely embedded in the face and has no osteological correlates; however, peripheral aspects of the sound producing mechanisms can leave traces on the skull and therefore can be inferred in fossils. Some of the facial air sacs, particularly the premaxillary air sac and the caudal air sacs, can sometimes form fossae on the skull. The large facial muscles that control the air sacs attach to a greatly expanded nasal process of the maxilla, which in odontocetes overlays most of the dorsal side of the frontal and temporal fossa. It has been suggested that the size of this process is correlated with the size and diversification of these muscles (Geisler et al. 2014, Sanders and Geisler 2015).

S3 – Previous work involving xenorophid cochlear morphology

Individual cochlear features (Park et al. 2016) support ultrasonic hearing in xenorophids, and principle components analyses (PCA) with linear measurements (Churchill et al., 2016) and 3D geometric morphometrics (Ekdale, 2016) discovered morphospaces separated all odontocetes (both living and extinct) from mysticetes and other outgroup taxa. Although Xenorophidae is a diverse clade, with 5 described genera (*Albertocetus*, *Cotylocara*, *Echovenator*, *Inermorostrum*, *Xenorophus*) and several more unnamed (Sanders and Geisler, 2015; Boessenecker et al., 2017a; Boessenecker et al. 2017b), it appears that the three studies on xenorophid cochlear morphology all sampled conspecific or congeneric taxa (Boessenecker et al., 2017b). It is crucial that inferences on the origin of echolocation based on these small samples be tested with data from other fossil odontocetes.

S4 – Detailed description of CCNHM 1000

Introduction

CCNHM-1000 is a small odontocete skull including partial premaxilla, maxilla, nasals, frontals, left lacrimal, left jugal, parietals, left alisphenoid, left squamosal, petrosals, left stapes, incus, and malleus, fragments of tympanic bullae, and five teeth and fragments.

Locality and Age

CCNHM 1000 was collected by James L. Goedert from near the mouth of Murdock Creek (Field Number JLG-76) on April 26, 1986. Calcareous siltstone concretions from this locality weather out from nearby exposures of the Oligocene Pysht Formation Clallam Co., Washington, USA (30.5–26.5 Ma; Prothero et al., 2001). These concretions have yielded a small assemblage including bivalves, gastropods, crinoids, plotopterid birds (*Tonsala hildegardae*, *Tonsala buchanani*), sleeper sharks (*Somniosus gonzalezi*), a desmostylian (*Behemotops proteus*), toothed mysticetes (cf. Mammalodontidae, *Fucaia buelli*), and the early diverging odontocete *Olympicetus avitus* (Olson, 1980; Domning et al., 1986; Goedert and Squires, 1993; Barnes and Goedert, 2001; Dyke et al., 2011; Welton and Goedert, 2016; Velez-Juarbe, 2017; Peredo et al., 2018; R.W. Boessenecker, pers. obs.). Marine mammals collected from other localities in the Pysht Formation include a possible record of the desmostylian *Kronokotherium*, the aetiocetid toothed baleen whale *Fucaia goedertorum*, an unnamed *Fucaia*-like aetiocetid, and the eomysticetid-like baleen whale *Sitsqwayk cornishorum* (Barnes et al., 1995; Peredo and Uhen, 2016; Marx et al., 2015).

The Pysht Formation consists of a 1.4 km thick succession of offshore mudrocks and sandy siltstones, and at its base includes turbidites; deposition likely ranged from 300-2000 m depths (Barnes and Goedert, 2001; Welton and Goedert, 2016). Magnetostratigraphic studies of the Pysht Formation assigned the unit to Chrons C11r-C8r, indicating an age of 30.5-26.5 Ma (late Rupelian to early Chattian; Prothero et al., 2001). A slightly younger age, 28.5-26.5 Ma, was assigned on the basis of finer age control to the Twin Rivers Quarry locality (=*Fucaia goedertorum* and *Sitsqwayk cornishorum* type localities) by Marx and Fordyce (2015, supplement). According to Domning et al. (1986) the Murdock Creek locality falls within the *Liracassis rex* mollusk zone, which has a minimum age of 29.5 Ma according to Prothero et al. (2001). However, these biozones are misleading (Nesbitt et al., 2010) and we adopt the more conservative age of 30.5-26.5 Ma.

Identification

CCNHM 1000 closely resembles *Olympicetus avitus* in the following suite of characters: rostrum wide at base, posterior wall of antorbital notch formed by maxilla, closely spaced buccal teeth, buccal teeth with labial and lingual cingula, lacrimal positioned below the frontal,

possessing a postorbital ridge, lacking a posterior maxillary foramen, ascending process of the maxilla reaching only to the posterior half of the supraorbital process of the frontal, nasals and premaxilla reaching only to anterior half of the supraorbital process of the frontal, posterolaterally oriented maxilla-frontal suture posterior to nasals, supraoccipital apex at same height as frontals/nasals, ventrally tapering postglenoid process, lacking an obvious tympanosquamosal recess, possessing a pit on the squamosal for the sigmoid process of the tympanic bulla, broad parietal exposure in the intertemporal region, lacking a sagittal crest, and possessing a concave posterior border of the supraorbital process of the frontal.

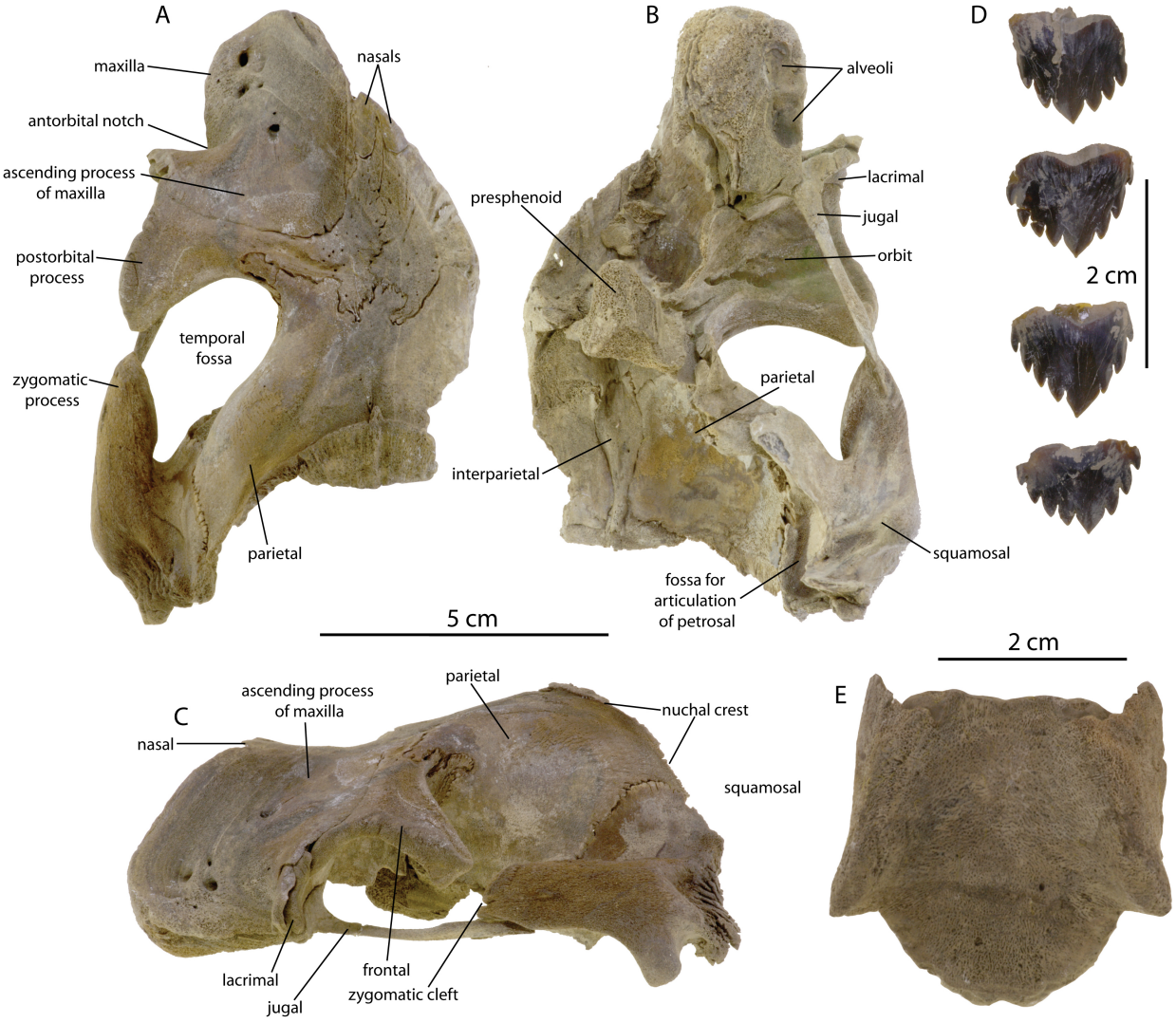

Figure S1. Morphology of the skull and teeth of CCNHM 1000, labeled.

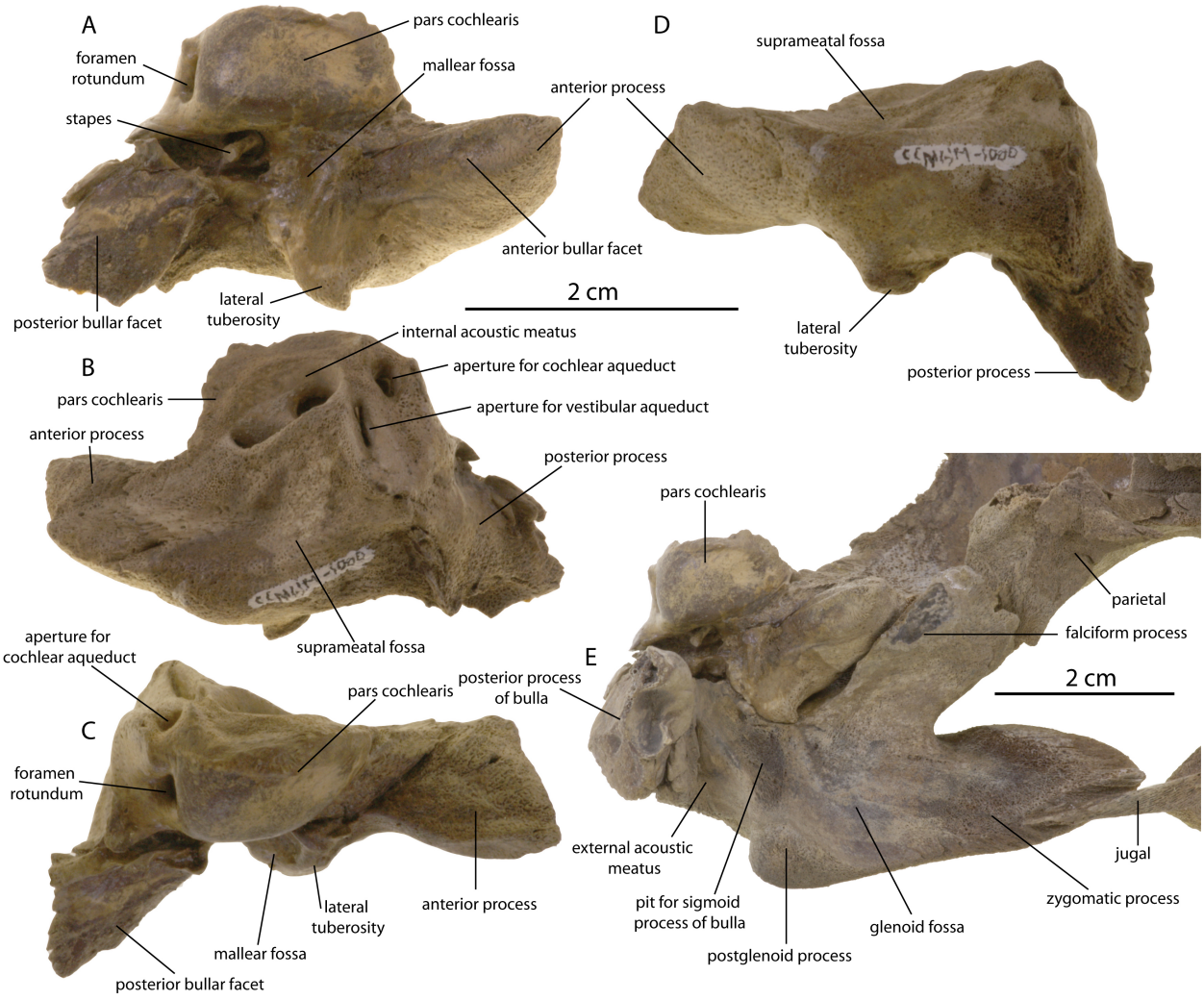

Figure S2. Morphology of the petrosal and its *in situ* position in CCNHM 1000, labeled.

Morphology of the skull of CCNHM 1000

CCNHM 1000 uniquely shares with *Olympicetus avitus* a transverse cleft in the apex of the zygomatic process of the squamosal, giving it a bifurcated outline in lateral view. Unless determined to be related to juvenile status of both specimens, this feature may be a potential autapomorphy of *Olympicetus*. However, CCNHM 1000 differs from *Olympicetus avitus* in possessing lower crowned cheek teeth with longer accessory cusps and more deeply incised interdental notches; the teeth are somewhat smaller in absolute size and exhibit more poorly developed labial cingulum. Owing to clear similarities with the holotype specimen and the possession of some differences in the dentition, we would like to identify CCNHM 1000 as *Olympicetus* sp., but refrain from doing so until better phylogenetic resolution is obtained.

Ontogenetic status – CCNHM 1000 represents a neonatal individual based on the unfused intersphenoidal and sphenoccipital synchondroses, persistent interparietal, unfused median frontal suture, limited dental development (enamel and minor mineralization of distal dentine shell of the roots), and small size (approximately 75% of the neonatal specimen LACM 126010).

Description – This description will focus on the morphology of this specimen that clearly differs from specimens published by Velez-Juarbe (2017) or on features not preserved in these published specimens, with an emphasis on the petrosal. The partial premaxilla that was preserved possesses a longitudinal sulcus similar to *Olympicetus avitus,* but not an obviously excavated premaxillary sac fossa. The premaxilla is incomplete, however, and so difficult to tell whether it is the right or left premaxilla (possibly right).

Vertex/skull roof: The anterolateral wing of the parietal does not extend quite as far laterally as in the holotype, where it reaches the transverse midpoint of the supraorbital process of the frontal, whereas in CCNHM 1000 it reaches approximately 40% of the distance from the midline. In CCNHM 1000 there is a tongue-shaped anterior invasion of the parietal between the left and right frontals, perhaps part of the interparietal that has dorsally fused to the parietals (see below). In CCNHM 1000 the posteriormost dorsal infraorbital foramen is positioned further posteriorly than the others and posterior to the antorbital notch; it is also positioned further dorsally, somewhat more derived than the condition in *Olympicetus avitus*.

Ventrally, within the braincase, a pair of clear sutures are present outlining a leaf-shaped interparietal. The interparietal is in turn divided into two portions separated by a small cleft: 1) a leaf-shaped anterior part which is anteroventrally flat and posteriorly transitions into a sub-cylindrical ridge posteriorly; 2) a posterior horizontal diamond-shaped plate with an articular surface dorsally with raised radial ridges for the supraoccipital. Anteriorly the interparietal contacts the frontals at the posterior end of the olfactory nerve tract.

The anterior and posterior portions of the interparietal are separated by a fine suture posteriorly at the termination of the median ridge (=falx cerebri). Dorsally, the parietal-interparietal suture is clearly visible along the left edge of the nuchal crest, with the medial 15 mm of the nuchal crest formed by the interparietal rather than parietal. The descending plate of the parietal is split into a medial sheet and a lateral sheet; the lateral sheet extends further

ventrally, and the two are separated by a narrow cleft that receives the medial plate of the alisphenoid.

Temporal Region: The posterolateral portion of the alisphenoid is "pinched" posteriorly and terminates to a point approximately 10mm anterior to the posterior edge of the temporal fossa, therefore forming the anterior portion of the subtemporal crest; the posterior 10mm of the blunt subtemporal crest is formed by the squamosal and parietal, and the squamosal-parietal suture runs along part of this crest. The posterior part of the alisphenoid is overlapped by both parietal (dorsally) and squamosal (ventrally).

The petrosal fossa is approximately triangular in outline and divided into a long, shallow anterior trough and a deeper posterior oval-shaped pit; the two are separated by a low, gently convex transverse ridge, similar to Xenorophidae. When placed in articulation with the squamosal, there is a narrow gap (1-3mm) between the anterior process of the petrosal and the falciform process of the squamosal. The petrosal only contacts the squamosal along the posterior margin of the lateral tuberosity, epitympanic hiatus (which receives the spiny process of the squamosal), and the lateral edge of the posterior process of the petrosal (articulating tightly with the posterior edge of the spiny process). Dorsolaterally a 2-4mm gap is present between the petrosal and squamosal. Fragments of a delicate medial sheet of the parietal articulate with the squamosal immediately dorsal to the petrosal fossa, and appear to have contacted or approximated the superior process or suprameatal fossa of the petrosal as in some well-preserved xenorophid basicrania (e.g. CCNHM 1838, Xenorophidae indet.).

Orbit: Unlike the holotype, CCNHM 1000 preserves a complete jugal in articulation with the rest of the skull. The jugals is delicate and strap-like with a lenticular cross-section; the anterior half is dorsoventrally compressed and the posterior half is transversely compressed. Anteriorly the jugal is not fused to the lacrimal; the jugal contacts the lacrimal ventrally and is in turn ventrally underlapped by the infraorbital plate of the maxilla. The anterior end of the jugal is 'hammer' shaped in ventral view owing to the anterior transverse expansion where it merges into the anteroventral surface of the orbit. The anterior end of the jugal is exposed ventrally but obscured laterally by the lacrimal. In lateral view, the ventral margin of the jugal is nearly

straight. The posterior end bears an elongate posterodorsally facing facet which articulates with the jugal facet on the anteroventral side of the zygomatic process of the squamosal.

Petrosal: The well-preserved petrosal bears a rectangular pars cochlearis, an elongate anterior process, a shallow supramastoid fossa, and a ventrally projecting posterior process. The anterior process is rectangular in medial and lateral view and slightly transversely narrower than dorsoventrally deep. A clear, flat anterior bullar facet is present, but a distinct fovea epitubaria is not developed. The anterointernal sulcus is deeply incised and runs from the medial edge of the mallear fossa anterodorsally toward the anterodorsal angle. An anteroexternal sulcus is not developed laterally and the lateral surface of the anterior process is smooth and continuous with the lateral surface of the petrosal body.

The lateral tuberosity is large and triangular, though somewhat shorter than in most Xenorophidae. Proximal to the tuberosity is a deeply excavated, circular mallear fossa. A small transverse ridge anterior to the fossa bears a small hook-like ridge to articulate with the accessory ossicle. Dorsally a shallow suprameatal fossa is present and extends anterior to the anterior incisure and posteriorly to about the level of the spiral cribriform tract. The suprameatal fossa is demarcated laterally by a low, transversely smooth, and laterally convex superior ridge. The pars cochlearis is rectangular in outline in ventral view and bears a low longitudinal ridge ventromedially. Anteriomedially the pars cochlearis bears short bladelike crests that run parallel with the shallow promontorial groove. The internal acoustic meatus is oval in shape and anterolaterally inclined; an anteroposteriorly oriented and sharp crista transversa is recessed 3mm inside the meatus, and divides the anterior part from a deep, circular spiral cribriform tract. The anterior part of the meatus consists of a deeply recessed and dorsally opening facial canal and foramen singulare; these foramina are separated by a low ridge. The meatus is not encircled by a raised ridge but the excavation of the suprameatal fossa has resulted in a sharp, crest-like lateral meatal rim. Posteriorly the aperture for the cochlear aqueduct is small, circular, and positioned immediately posterior to the spiral cribriform tract; a small tubercle is present between these two foramina. The aperture for the vestibular aqueduct is nearly transversely oriented and developed as an anteroposteriorly compressed fissure. Just anterior is a sharp crest that rises to a conical projection (=posterodorsal angle of Boessenecker and Fordyce 2015). The fenestra cochleae is D-shaped and immediately dorsomedial is a low tubercle. A tongue-shaped,

transversely narrow, and bladelike posterior cochlear crest is present and plunges posteroventrally; it roofs over a deeply excavated stapedial muscle fossa which is not clearly separated from the facial sulcus. A transversely narrow slot its present between the posterior cochlear crest and the shallow, small stylomastoid fossa.

The posterior process is directed nearly ventrally and the posterior margin forms a right angle relative to the superior ridge in medial view. The posterior bullar facet is smooth, diamond-shaped, transversely convex, and slightly longitudinally concave. Medially a tongue-like facial crest projects ventromedially from the facet. Anteriorly, a small, trough-like incudal fossa is developed and leads anteriorly to a sharp crest on the lateral margin of the facial sulcus. A low, transversely oriented articular rim is present along the base of the posterior process, but it is not hook-like as in Platanistoidea.

The petrosal of CCNHM 1000 shares two features that Park et al. (2016) considered to be synapomorphies of the Xenorophidae: 1) a transversely compressed anterior process and 2) a triangular lateral tuberosity that is somewhat enlarged. Regarding the first feature, the anterior process in CCNHM 1000 is somewhat less compressed than in xenorophids (e.g. *Albertocetus*, *Cotylocara*, *Echovenator*) and broadly similar to that of *Agorophius* (Godfrey et al., 2016). This is the primitive condition for odontocetes. Regarding the second feature, the lateral tuberosity is perhaps less elongate than in most published xenorophids but the triangular shape is genuinely shared to the exclusion of most other odontocetes.

CCNHM 1000 differs from xenorophids in possessing a larger and shallow suprameatal fossa with indistinct margins and by possessing an anterior bullar facet (which it shares with all later diverging odontocetes). Amongst odontocetes, suprameatal fossae are present only in CCNHM 1000 and Xenorophidae. CCNHM 1000 compares quite well with *Simocetus rayi*, differing only in having a triangular lateral tuberosity; the dorsal surface of the periotic of *Simocetus* is not yet known since it is still embedded in concretionary matrix (Fordyce, 2002). CCNHM 1000 further differs from xenorophids in lacking a long posterior cochlear crest, lacking a transversely swollen superior process with fine sulci, and by lacking a hatchet-shaped anterior process with a spine-like anterodorsal angle.

Dentition: Only postcanine teeth are preserved; one triangular anterior cheek tooth is preserved along with four posterior molariform teeth and fragments. The position of teeth in CCNHM 1000

and the holotype is unclear. The anterior cheek tooth has a smooth and sharp anterior carina, and a similar posterior carina but with a single basal cusp. The molariform cheek teeth are consistently lower crowned than in the holotype specimen; in CCNHM 1000 the apicobasal height:anteroposterior length ratio is 9.16:13mm (70%) whereas the lowest crowned teeth of the holotype has a height:length ratio of 16.4:17mm (96%). In absolute size, the teeth of CCNHM 1000 are approximately 80% of the anteroposterior length of the holotype. The accessory cusps of the molariform teeth are identical in count but are more acutely triangular. When measuring the angle between the intercusp notches and cusp tips, the apicalmost cusps of molariform teeth in CCNHM 1000 exhibit angles between 44.7 and 55.4°; in the holotype these angles range from 78-87°, reflecting blunter cusps and shallower notches.

Specimen measurements:

Skull width at antorbital notch: 46.0 mm
Skull width at postorbital process: 99.2 mm
Skull width at zygomatic process apex: 92.0 mm
Maximum squamosal width: 109.0 mm
Transverse width of nasals (as preserved): 11.4 mm
Interorbital width: 93.8 mm
Maximum anteroposterior length of orbit: 29.4 mm
Maximum height/depth of orbit: 20.0 mm
Maximum anteroposterior length of parietal exposure at midline: 32.1 mm
Ascending maxilla, maximum transverse width (left): 36.2 mm
Ascending maxilla (left), maximum anteroposterior length from antorbital notch: 29.2 mm
Height of nasals above lateral edge of rostrum: 43.4 mm
Least intertemporal width: 38.6 mm
Depth of squamosal fossa: 8.5 mm
Transverse width between deepest point of squamosal fossa and supramastoid crest: 7.0 mm
Anteroposterior length, zygomatic process to postglenoid process:45.6 mm
Transverse width of glenoid fossa: 16 mm
Transverse width across basioccipital crests: 37.4 mm
Petrosal, total length: 40.0 mm

Pars cochlearis length (ant margin to fenestra cochleae/rotundum): 15.3 mm
Pars cochlears transverse width (medial edge to fenestra ovalis): 9.2 mm
Length of anterior process: 12.8 mm
Anterior process, transverse width at midpoint: 8.7 mm
Anterior process, dorsoventral depth at midpoint: 12.1 mm
Separation between fenestra rotundum/cochleae and cochlear aqueduct: 3.3 mm
Separation between fenestra rotundum/cochleae and vestibular aqueduct: 6.5 mm
Separation between fenestra ovalis and fenestra cochleae/rotundum: 5.3 mm
Posterior bullar facet, anteroposterior length: 14.6 mm
Posterior bullar facet, transverse width: 9.6 mm
Suprameatal fossa, anteroposterior length: 19.0 mm
Suprameatal fossa, transverse width: 8.9 mm
Postcanine A, apicobasal length/mesiodistal length/transverse width: 10.0/ 13.7/5.3 mm
Postcanine B, apicobasal length/mesiodistal length/transverse width: 12.3/14.3/5.1 mm
Postcanine C, apicobasal length/mesiodistal length/transverse width: 11.7/?/5.2 mm
Postcanine D, apicobasal length/mesiodistal length/transverse width: 12.4/13.6/5.5 mm

S5 – PCA

Measurements acquired were: cochlear length (Cl), secondary bony lamina length (SBL), cochlear width (Cw), cochlear width perpendicular to Cw (W2), inter-turn distance (ITD), spiral ganglion canal width at the first quarter-turn (GAN), surface area of the fenestra cochleae (FC), and number of turns (T). The PCA was performed using the FactoMineR package (Le et al., 2008) in the R programming language (R Core Team, 2015). Following Mourlam and Orliac (2017), any measurements that could not be taken from the CT scans were imputed using the missMDA package (Josse & Husson, 2016), although missing data were very few (Data Table S1). Rotational head movement sensitivity of CCNHM 1000 was estimated using '90var' (Malinzak et al., 2012; Berlin et al. 2013). An alternative PCA excluding some monodontid data was performed to provide a less complex visualization of the data (Fig. S3; Data Table S2).

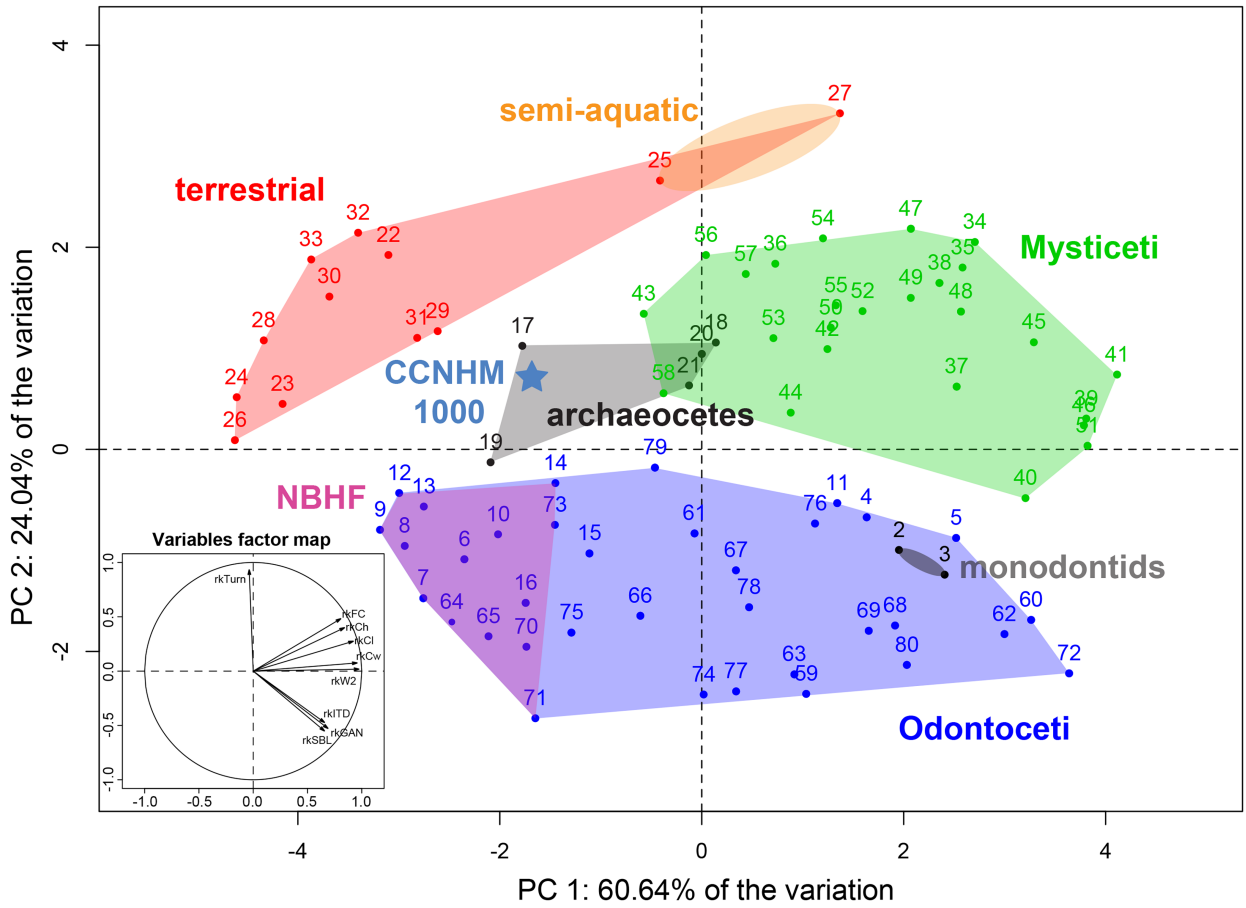

Figure S3. Principle components analysis excluding some monodontids (data file used included in ESM, DataTableS2_excludingmonodontids.csv). Numbers associated with specific taxa are listed in the Data Table S2 provided as a separate file.

S6 – Semicircular canal measurements used to calculate 90var, and calculated results

Correlates for ecological preference – To obtain relevant information on the rotational head movement sensitivity of CCNHM 1000, we used a method independent of body size, '90var' (Malinzak et al., 2012; Berlin et al. 2013), that has been used with some success in cetaceans (Ekdale & Racicot, 2015; Racicot et al. 2016; Racicot et al. 2018; but see Costeur et al. 2018). 90var is calculated as the absolute value of the deviation from 90^{o} of each angle between ipsilateral semicircular canals. The resulting value is negatively correlated with head movement sensitivity (Berlin et al. 2013 and Malinzak et al. 2012) whereby smaller 90var values are expected to indicate higher sensitivity to head movements, which is associated with faster movement or more agility. The ipsilateral semicircular canal angles of CCNHM 1000 were measured using planes manually inserted through the canals with the "Oblique Slice" module in

Avizo ("plane method", *sensu* Racicot et al. 2018; S2). For accuracy each measurement was repeated three times for each angle and averaged before calculating 90var.

Table S1. Measurements of the semicircular canal angles.

		Canal Angles			Canal Deviations			
Taxon	**Museum Number**	**A-L**	**A-P**	**L-P**	**90A-L**	**90A-P**	**90L-P**	**90var**
Olympicetus sp.	CCNHM 10000	99	96.7666667	91.3333333	9.00	6.77	1.33	5.70

S7 - Phylogenetic reconstruction

Sixteen most parsimonious trees were found using the application TNT (Goloboff et al. 2008), using default settings under a "New Technology Search" except for setting the minimum length to be found 1000 times. Lengths of the most parsimonious trees were 4173236. All most parsimonious trees reconstruct CCNHM 1000 as sister to a clade including odontocetes more closely related to and including Crown odontocetes, as reflected by the strict consensus tree (Fig. S4). Support for clades was assessed using the bootstrap with replacement in TNT, although unlike default settings, absolute frequencies are reported and 50 random taxon addition sequences were used for each bootstrap replicate. Bootstrap support values for nodes are shown on the strict consensus tree.

Our phylogenetic analysis placed CCNHM 1000 in a clade of all odontocetes except xenorophids, *Archaeodelphis patrius*, and *Ashleycetus planicapitis* (S7). This clade is supported by five synapomorphies in all most parsimonious trees: base of rostrum slightly bowed (character 12, 0 > 1), occipital bears sagittal crest (156, 0 > 1), petrosal lacks groove for capsuloparietal vein (207, 0 > 1), deep anterior bullar facet on petrosal (210, 1 > 3), and posterior process of bulla has few laminations (264, 1 > 0). The first of these synapomorphies also occurs in xenorophids, but is here interpreted as convergent based on a fairly straight rostrum in *Archaeodelphis* and the unnamed taxon represented by ChM PV4746. CCNHM 1000, *Olympicetus avitus*, and *Mirocetus riabinini* appear to represent a similar grade of basal odontocete; all are excluded from a clade that includes crown odontocetes and many extinct forms, such as *Agorophius pygmaeus*. This clade is supported by three synapomorphies: loss of infraorbital plate (60, 1 > 0), premaxilla terminates over orbit (75, 1 > 3 or 4), and supraoccipital reaches level of zygomatic process (140, 0 > 1).

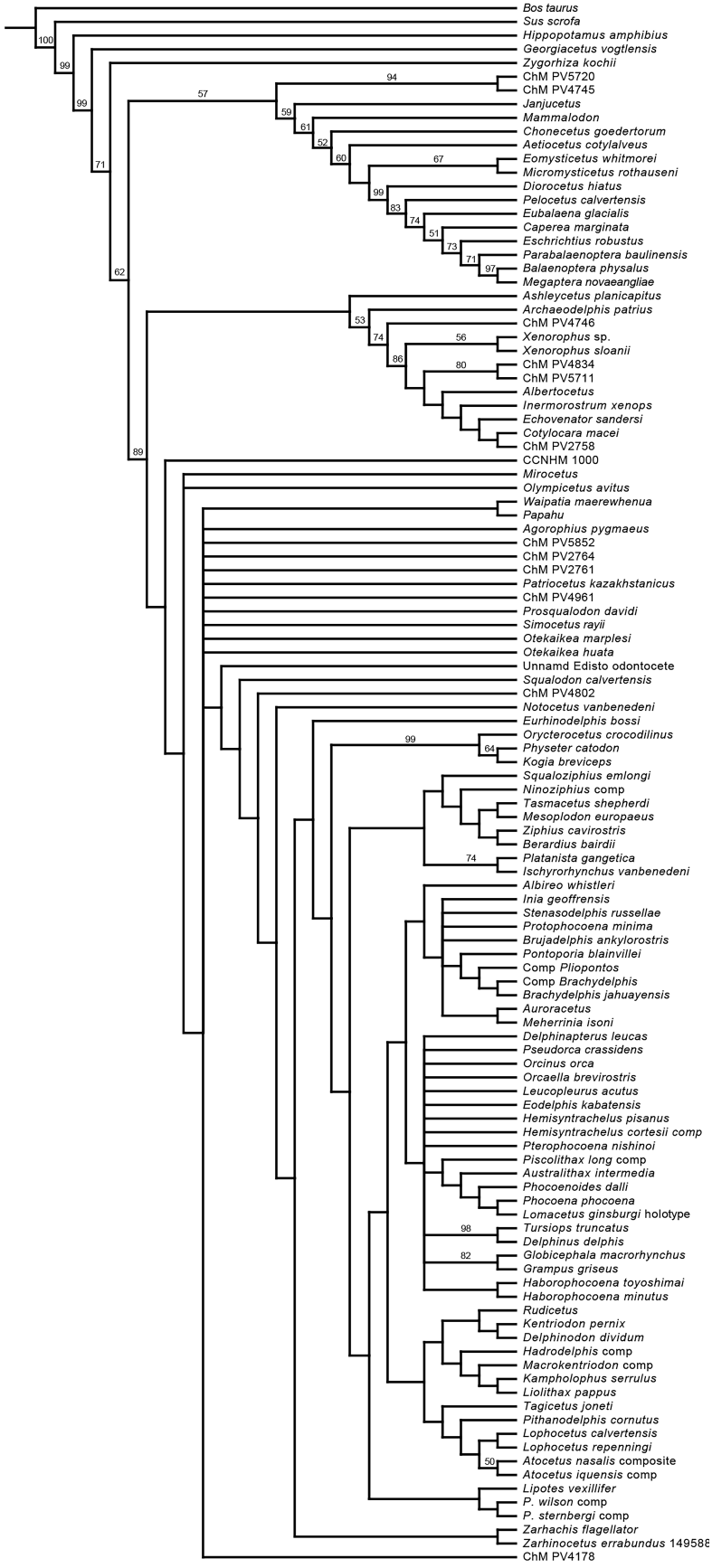
Bos taurus
Sus scrofa
Hippopotamus amphibius
Georgiacetus vogtlensis
Zygorhiza kochii
ChM PV5720
ChM PV4745
Janjucetus
Mammalodon
Chonecetus goedertorum
Aetiocetus cotylalveus
Eomysticetus whitmorei
Micromysticetus rothauseni
Diorocetus hiatus
Pelocetus calvertensis
Eubalaena glacialis
Caperea marginata
Eschrichtius robustus
Parabalaenoptera baulinensis
Balaenoptera physalus
Megaptera novaeangliae
Ashleycetus planicapitus
Archaeodelphis patrius
ChM PV4746
Xenorophus sp.
Xenorophus sloanii
ChM PV4834
ChM PV5711
Albertocetus
Inermorostrum xenops
Echovenator sandersi
Cotylocara macei
ChM PV2758
CCNHM 1000
Mirocetus
Olympicetus avitus
Waipatia maerewhenua
Papahu
Agorophius pygmaeus
ChM PV5852
ChM PV2764
ChM PV2761
Patriocetus kazakhstanicus
ChM PV4961
Prosqualodon davidi
Simocetus rayii
Otekaikea marplesi
Otekaikea huata
Unnamd Edisto odontocete
Squalodon calvertensis
ChM PV4802
Notocetus vanbenedeni
Eurhinodelphis bossi
Orycterocetus crocodilinus
Physeter catodon
Kogia breviceps
Squaloziphius emlongi
Ninoziphius comp
Tasmacetus shepherdi
Mesoplodon europaeus
Ziphius cavirostris
Berardius bairdii
Platanista gangetica
Ischyrorhynchus vanbenedeni
Albireo whistleri
Inia geoffrensis
Stenasodelphis russellae
Protophocoena minima
Brujadelphis ankylorostris
Pontoporia blainvillei
Comp Pliopontos
Comp Brachydelphis
Brachydelphis jahuayensis
Auroracetus
Meherrinia isoni
Delphinapterus leucas
Pseudorca crassidens
Orcinus orca
Orcaella brevirostris
Leucopleurus acutus
Eodelphis kabatensis
Hemisyntrachelus pisanus
Hemisyntrachelus cortesii comp
Pterophocoena nishinoi
Piscolithax long comp
Australithax intermedia
Phocoenoides dalli
Phocoena phocoena
Lomacetus ginsburgi holotype
Tursiops truncatus
Delphinus delphis
Globicephala macrorhynchus
Grampus griseus
Haborophocoena toyoshimai
Haborophocoena minutus
Rudicetus
Kentriodon pernix
Delphinodon dividum
Hadrodelphis comp
Macrokentriodon comp
Kampholophus serrulus
Liolithax pappus
Tagicetus joneti
Pithanodelphis cornutus
Lophocetus calvertensis
Lophocetus repenningi
Atocetus nasalis composite
Atocetus iquensis comp
Lipotes vexillifer
P. wilson comp
P. sternbergi comp
Zarhachis flagellator
Zarhinocetus errabundus 149588
ChM PV4178

Figure S4 (previous page). Strict consensus tree of 16 most parsimonious trees. Values at nodes represent bootstrap support values of 50% and above.

S8 – Character mappings of commonly used hearing-related traits of the cochlea.

Characters and optimization: Following Mourlam & Orliac (2017), scaled inter-turn distance (ITD) was calculated as a fraction of the surface area of the fenestra cochleae (ITD/FC), basal ratio (BR) was calculated as cochlear height divided by cochlear width, relative spiral ganglion width GAN was calculated as a percentage of the surface area of the fenestra cochleae, SBL was calculated as a fraction of the cochlear length, and number of turns was calculated using cochlear coiling, i.e., the number of turns of the cochlea calculated using Coil–96 (originally described by Geisler & Luo 1996, named in Ekdale & Rowe 2011). Because of the continuous nature of these characters, the character states were binned into as many discrete characters as possible (up to 9) to investigate finer levels of character state sampling before performing ancestral character state reconstructions. Character states were binned by first normalizing all measured values between 0 and 1. Characters were then binned by dividing into 9 equal bins (9 is the maximum allowed for discrete character tracings). Based on this equal apportionment, some states weren't occupied, resulting in a lower number (than 9) of unique character states. Ancestral character state reconstructions of individual ordered characters was performed in Mesquite v. 3.03

Trees used: Characters were mapped onto two distinct agreement subtrees that result from pruning taxa that lack scorings for these inner ear characters (16 most parsimonious trees resolve to 2 distinct trees when taxa are deleted). We have used the agreement subtrees for clarity and ease of visualization. All taxa deleted did not have scorings for the inner ear characters (i.e., they were coded as "?"), so the ancestral character state reconstructions are not changed by this pruning. These reconstructions are compatible with those based on trees that include all taxa, but are easier to visualize. The exclusion of taxa that lacked the scorings reduced 16 most parsimonious trees to two distinct trees, which varied in the position of the stem phocoenid *Pterophocoena nishinoi*. The NEXUS file used for tracings is provided as an additional file in the supplemental material (CCNHM_1000_pruned_trees.nex).

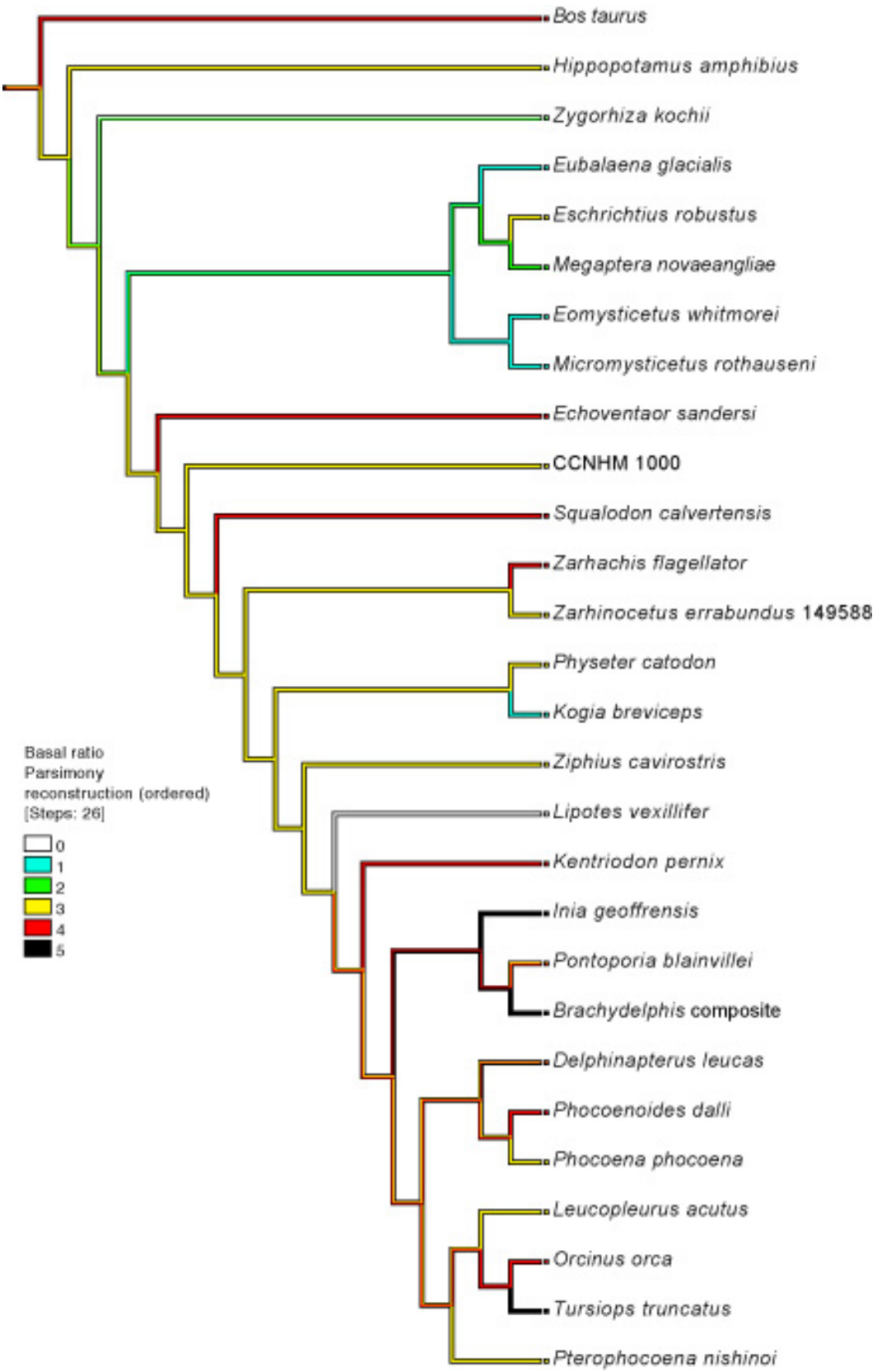

Figure S5. Character mapping of the basal ratio of the cochlea on agreement subtree 1.

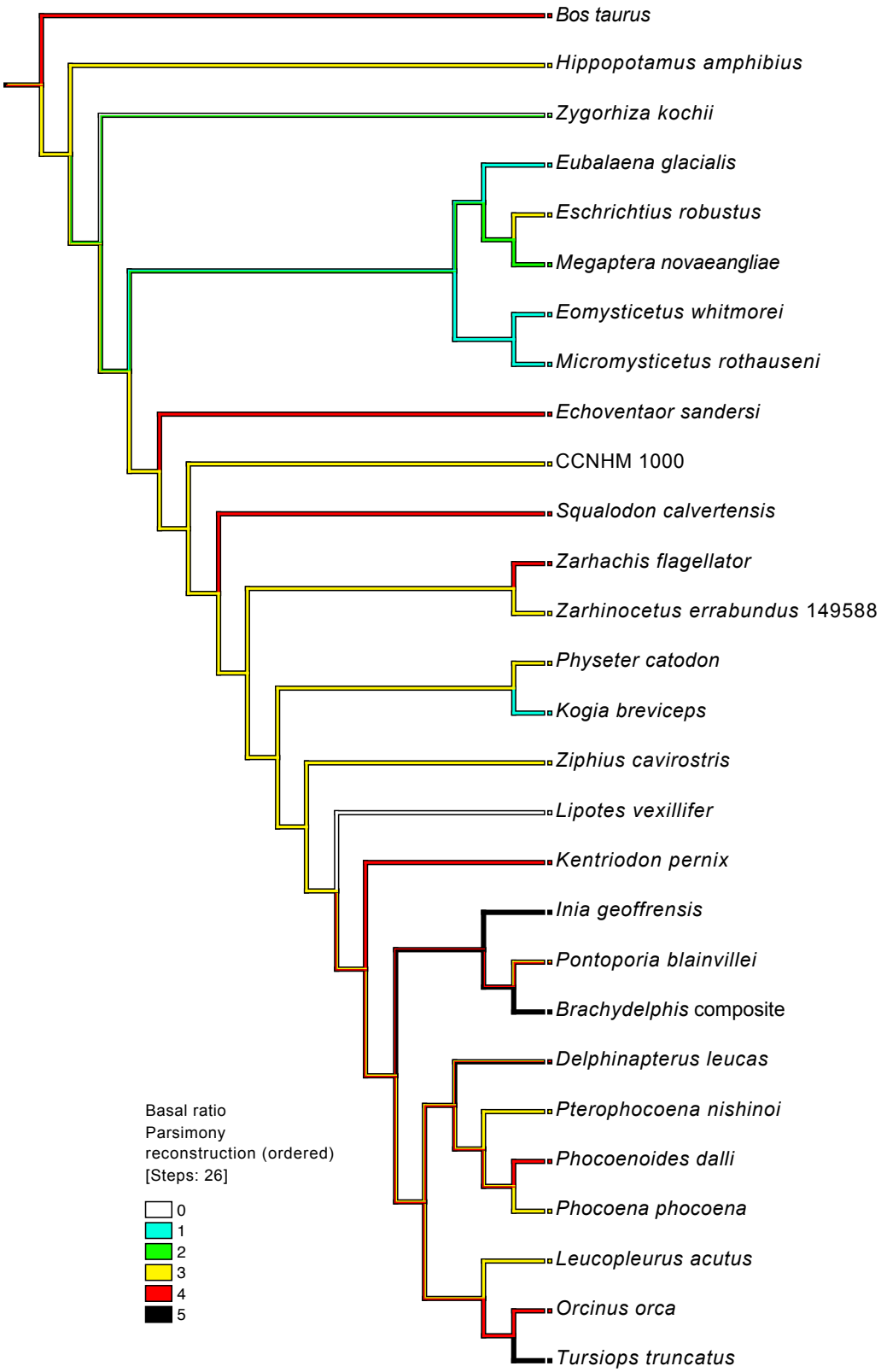

Figure S6. Character mapping of the basal ratio of the cochlea on agreement subtree 2.

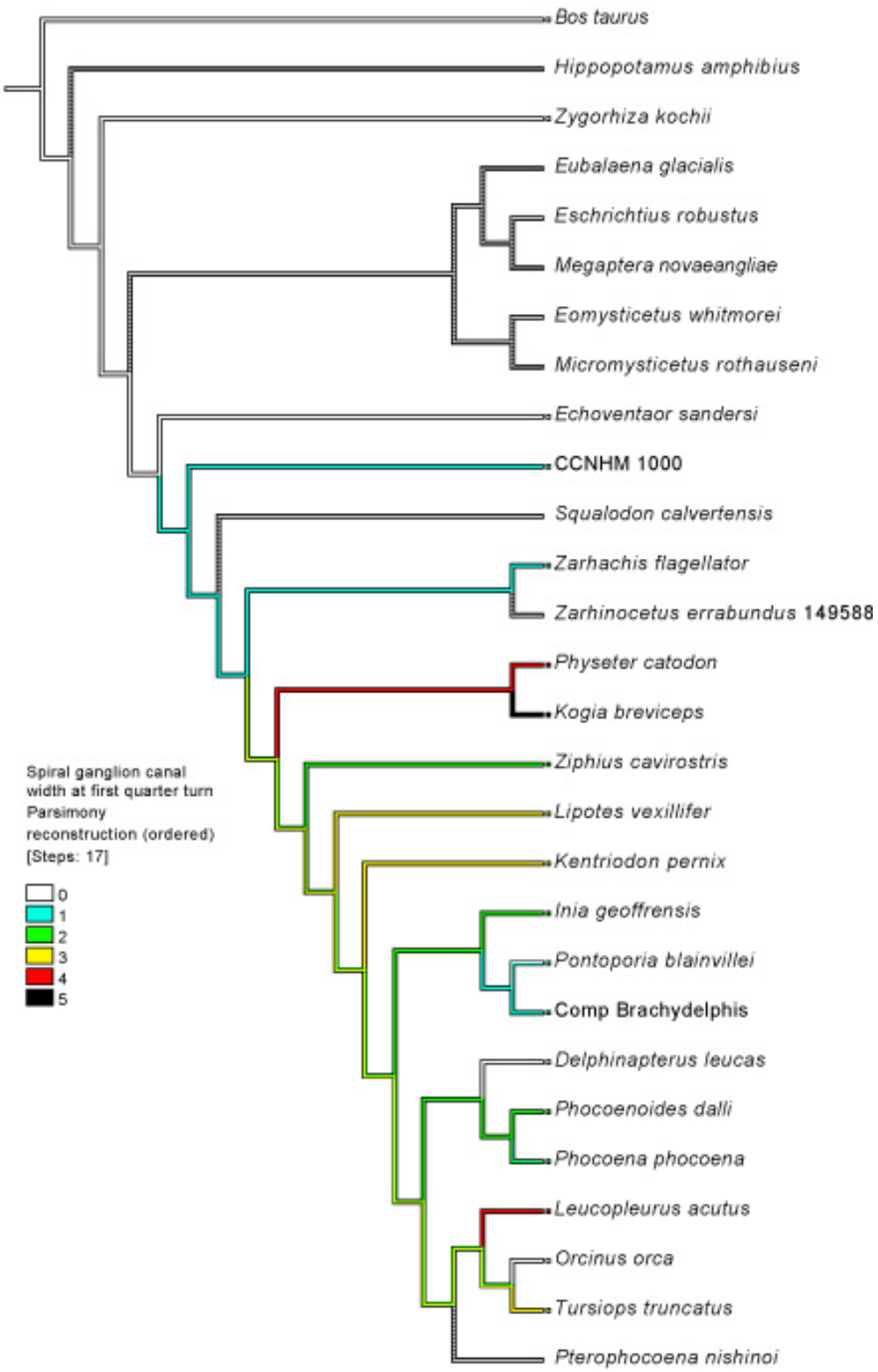

Figure S7. Character mapping of spiral ganglion canal width at first quarter turn of the cochlea on subtree 1.

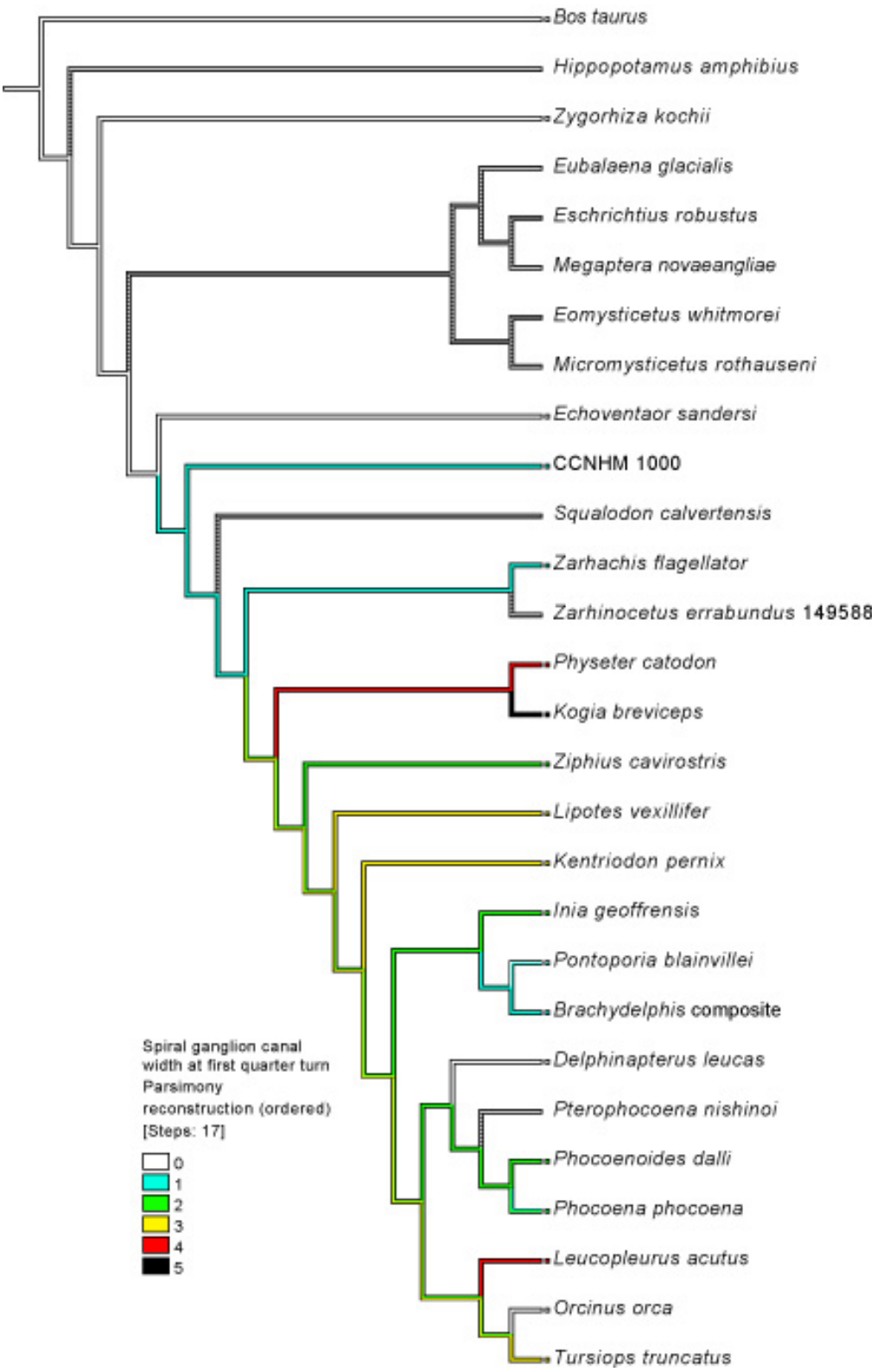

Figure S8. Character mapping of spiral ganglion canal width at first quarter turn of the cochlea on subtree 2.

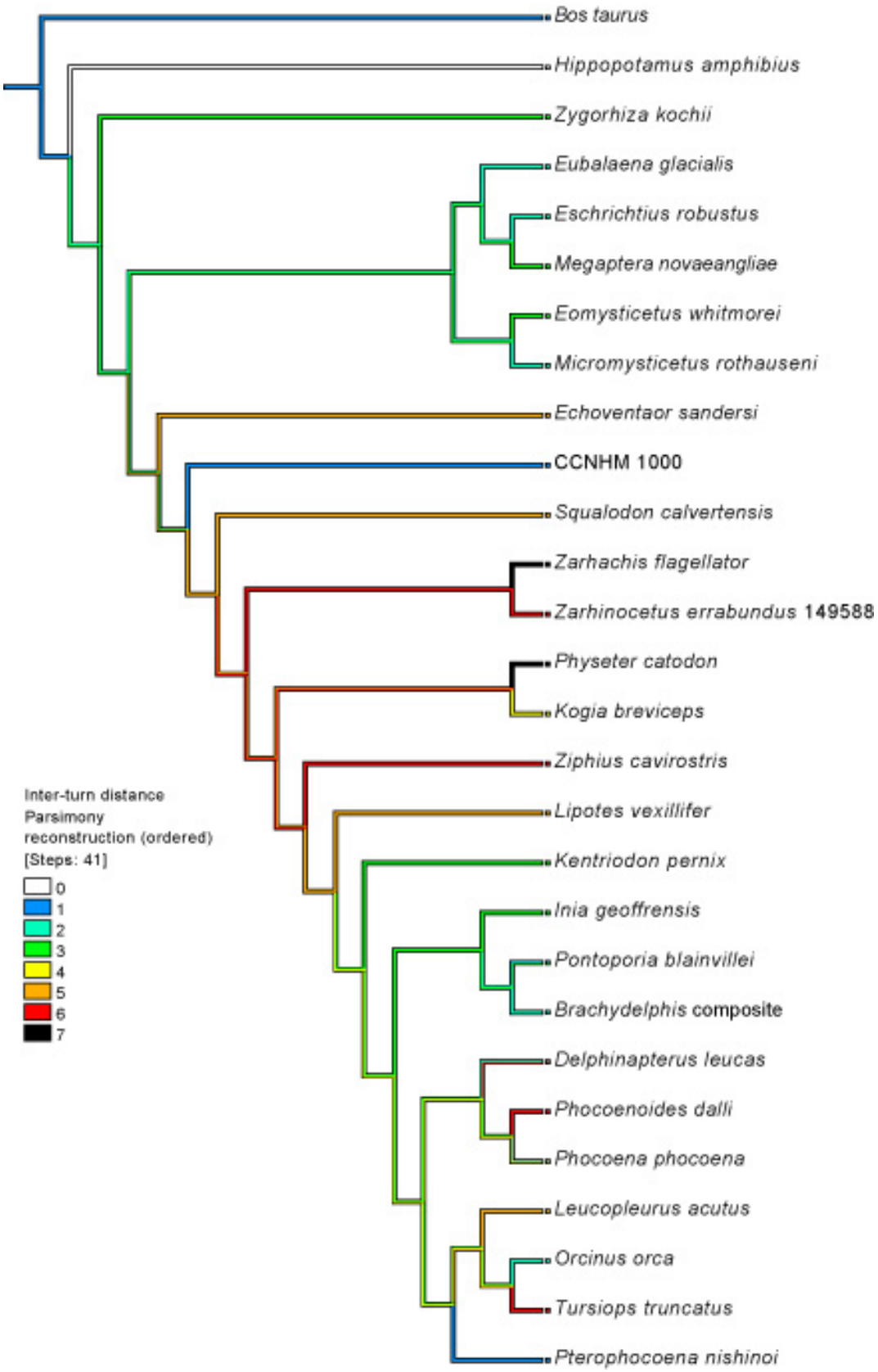

Figure S9. Character mapping of inter-turn distance on agreement subtree 1.

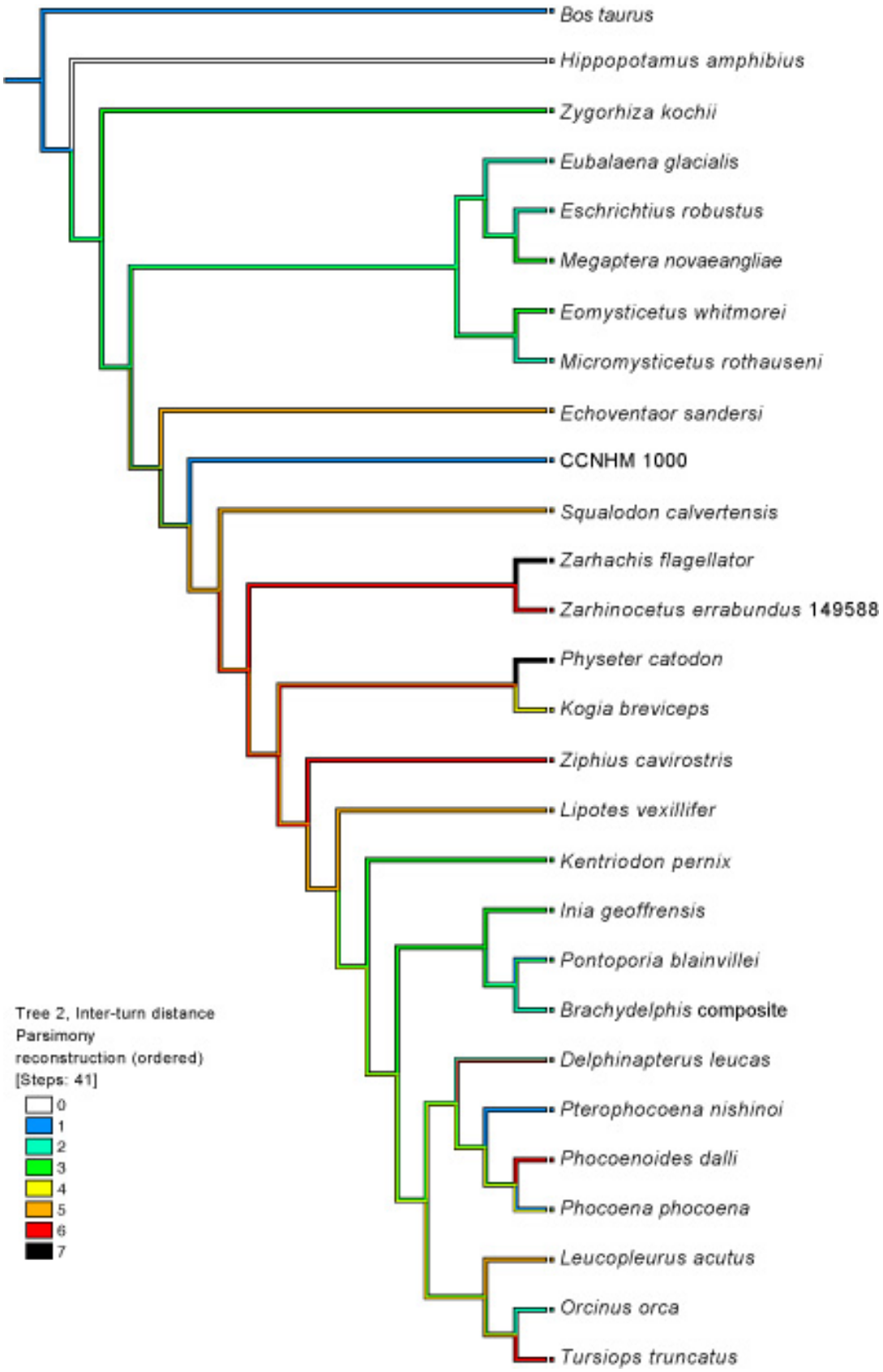

Figure S10. Character mapping of inter-turn distance on agreement subtree 2.

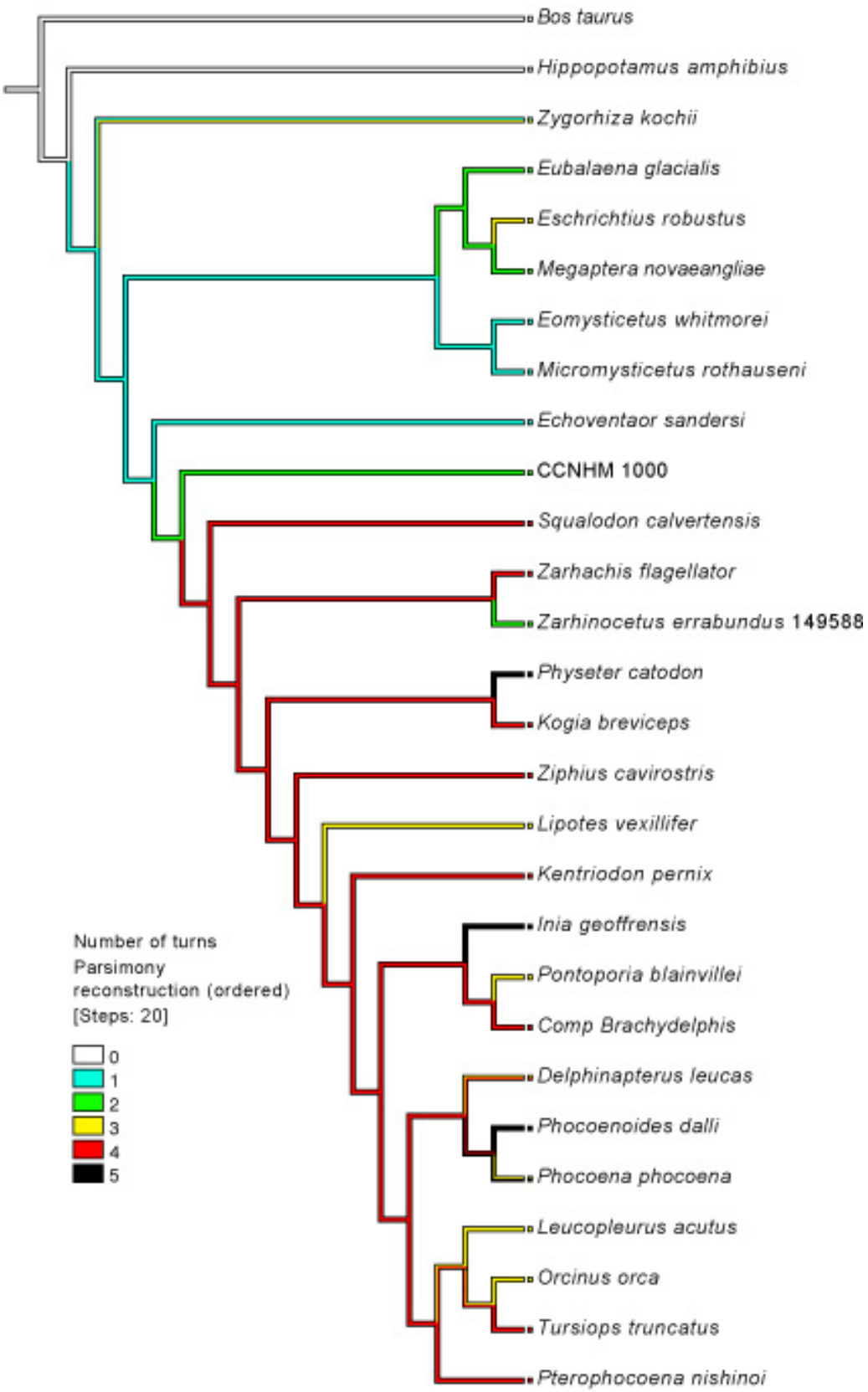

Figure S11. Character mapping of number of turns of the cochlea on agreement subtree 1.

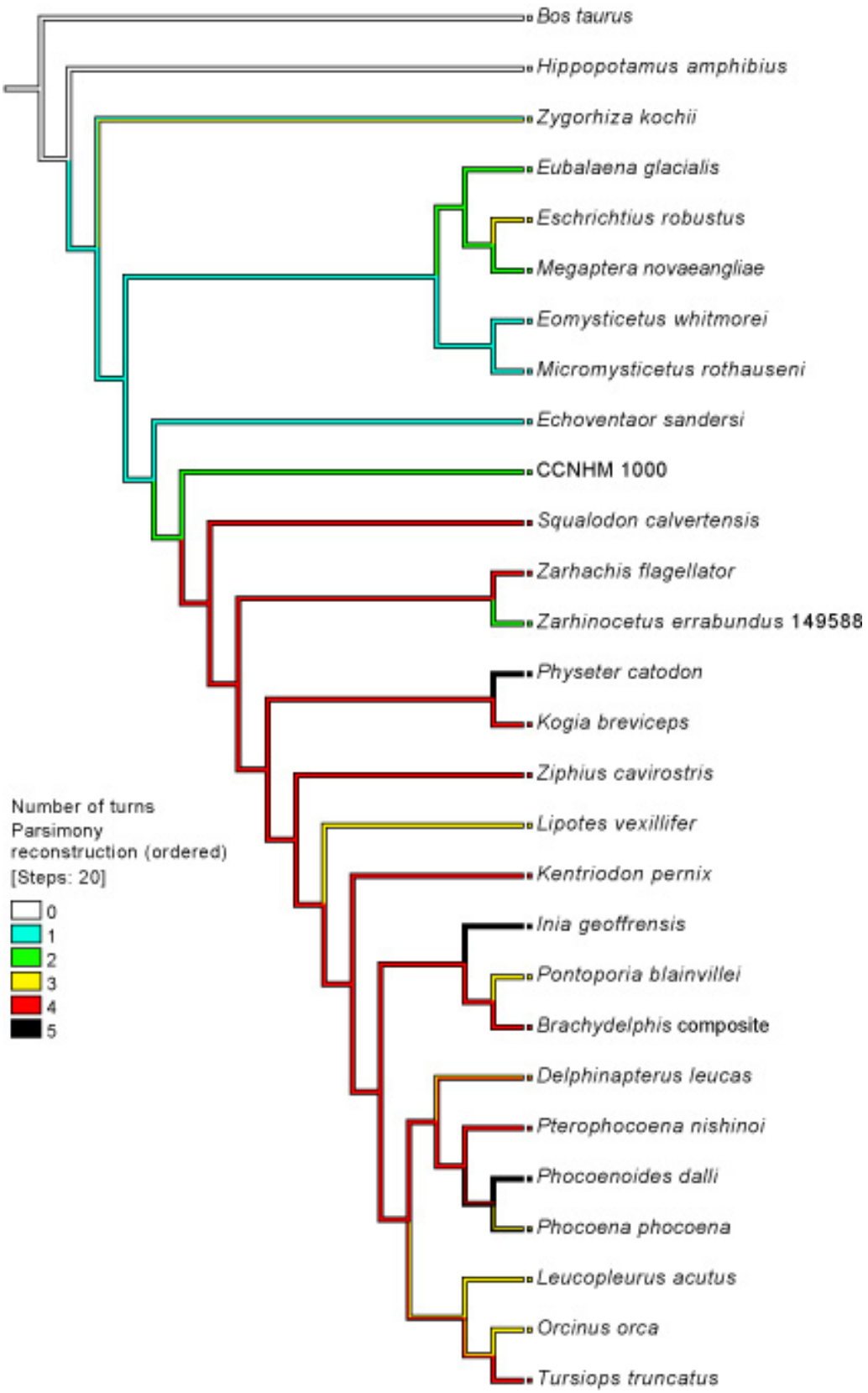

Figure S12. Character mapping of number of turns of the cochlea on agreement subtree 2.

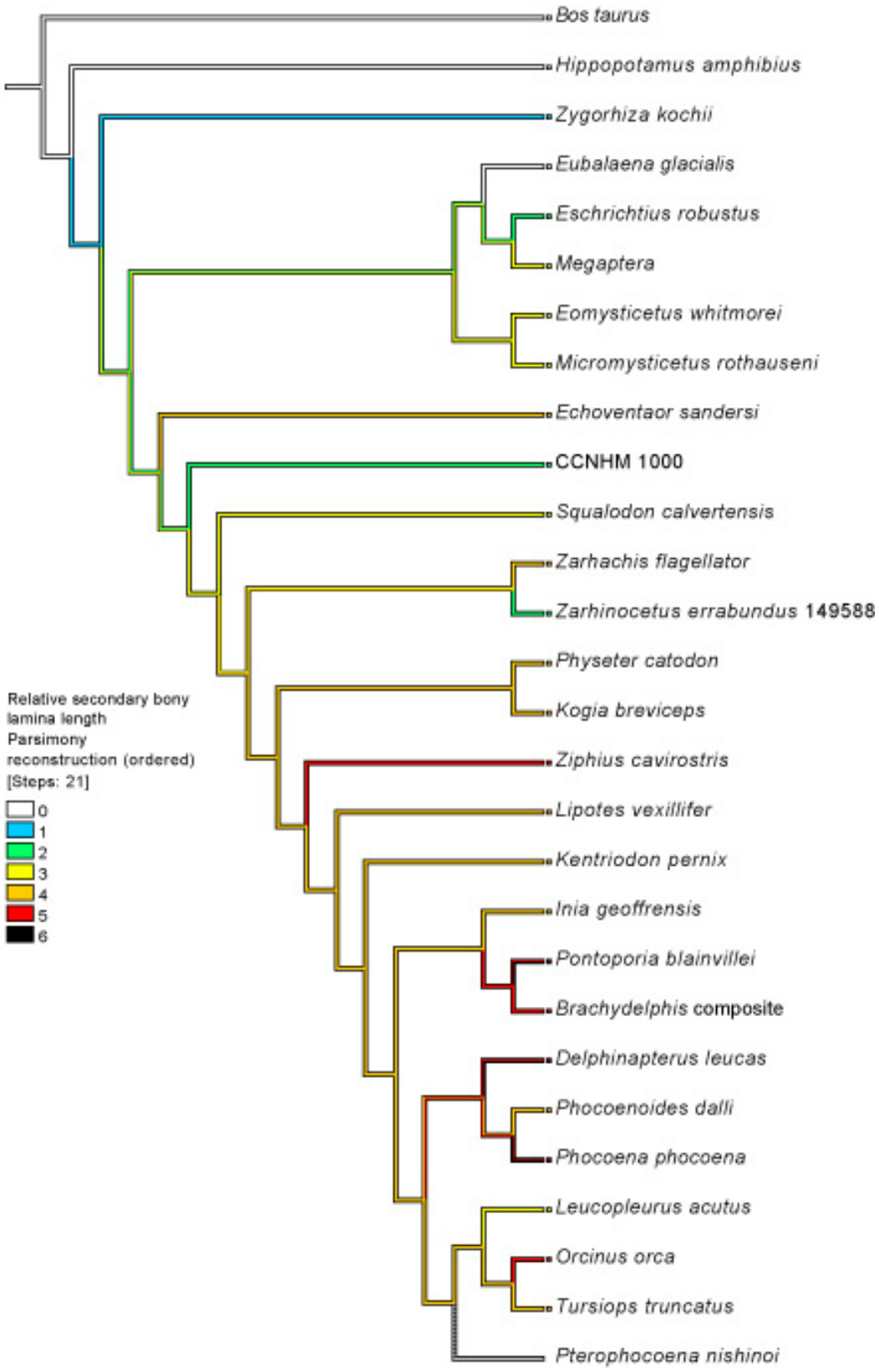

Figure S13. Character mapping of secondary bony lamina length as percentage of cochlear length on subtree 1.

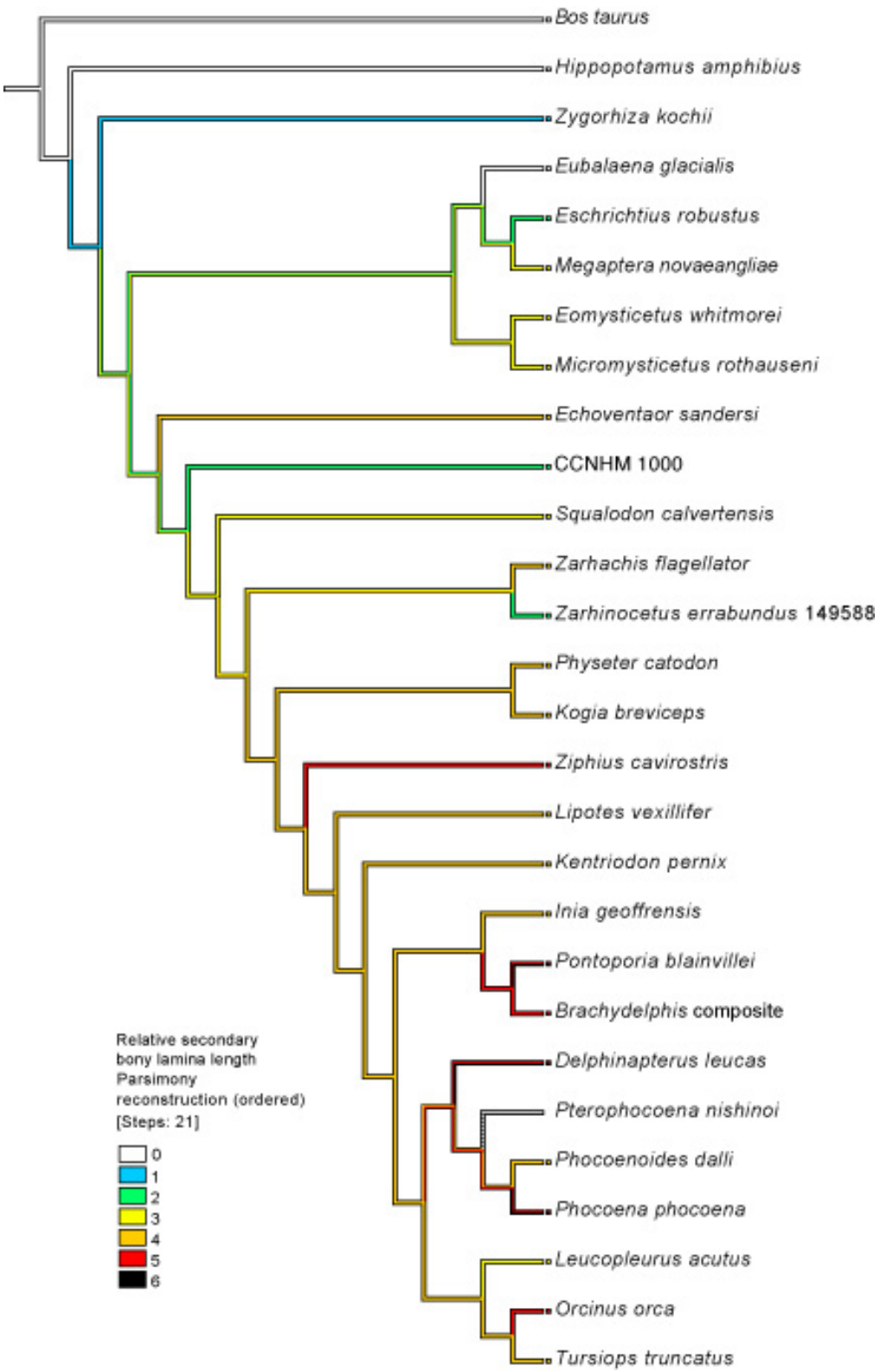

Figure S14. Character mapping of secondary bony lamina length as percentage of cochlear length on subtree 2.

S9 – Detailed specimen identification

The characters by which CCNHM 1000 resembles *Olympicetus avitus* are as follows: rostrum wide at base, posterior wall of antorbital notch formed by maxilla, closely spaced buccal teeth, buccal teeth with labial and lingual cingula, lacrimal positioned below the frontal, postorbital ridge present, absence of a posterior maxillary foramen, ascending process of the maxilla reaching only to the posterior half of the supraorbital process of the frontal, nasals and premaxilla reaching only to anterior half of the supraorbital process of the frontal, posterolaterally oriented maxilla-frontal suture posterior to nasals, supraoccipital apex at same height as frontals/nasals, ventrally tapering postglenoid process, absence of tympanosquamosal recess, presence of a pit on the squamosal for the sigmoid process of the tympanic bulla, broad parietal exposure in the intertemporal region, absence of a sagittal crest, and concave posterior border of the supraorbital process of the frontal (Veléz–Juarbe, 2017; S4).

CCNHM 1000 uniquely shares with *Olympicetus avitus* a transverse cleft in the apex of the zygomatic process of the squamosal, giving it a bifurcated outline in lateral view. However, CCNHM 1000 differs from *Olympicetus avitus* in possessing teeth that are somewhat smaller in absolute size, are lower crowned, have a weaker labial cingulum, have higher accessory cusps, and have deeper notches between cusps (S4). Owing to clear similarities with the holotype specimen yet the occurrence of differences in the dentition, CCNHM 1000 we would identify *Olympicetus* sp. (for complete formal description see S4), but have chosen to refrain from identification at this stage.

S10 – Detailed bony labyrinth morphology

CCNHM 1000 has a much smaller inter-turn distance at the first quarter turn (0.57 mm), i.e., in the basal region of the cochlea, than *Echovenator* (1.56 mm) and cf. *Cynthiacetus* (1.45 mm), although other archaeocetes/protocetids range from 0.9 mm to 1.2 mm (Data Table S1). The secondary bony lamina occupies 55.32% of the cochlear length (Data Table S1), although it may be slightly longer as matrix fills the cochlea above this point. The basal ratio is 0.46, meaning that the length of the axis of the spiral is roughly less than half the diameter of the basal turn. This value is in the middle range of our sample, which varies from 0.34 in the small extinct odontocete *Pliopontos littoralis* to 0.83 in the extinct cetothere (mysticete) *Metopocetus durinasus*. Specimens with similar basal ratios include *Delphinapterus leucas*, *Phocoena*

phocoena, *Acrophyseter*, and *Aulophyseter morricei*. Internally, the width of the spiral ganglion canal at the first quarter turn is 0.55 mm, similar to values of narrow-band, high-frequency specialists such as *Pontoporia blainvillei, Pterophocoena nishinoi*, *Kentriodon pernix*, *Kogia sima*, and other taxa which have smaller body sizes (Galatius et al. 2018). It is also similar to a measurement from a *Zygorhiza kochii* specimen (0.6 mm) and some mysticetes (*Balaenoptera acutorostrata*, "*Balaenoptera" ryani, Micromysticetus rothauseni*, and *Peripolocetus vexillifer*, Data Table S1).

The vestibule and semicircular canals appear relatively large compared to the cochlea (Fig. 1, Fig. S16). The vestibular complex (including semicircular canals but excluding the aqueductus vestibuli) makes up 14.77% of the total volume of the bony labyrinth (21.77 cubic mm vs. 147.98 cubic mm). The cochlear volume of CCNHM 1000 (122.35 cubic mm) makes up 83% of the whole bony labyrinth, which is within the range found for extinct and extant baleen whales (75%–91%) and stem odontocetes (82–85%) although somewhat low compared with crown odontocetes (88%) (Ekdale 2016). Crown odontocetes with relatively small vestibular complexes, such as porpoises (Phocoenidae) range in percentage cochlear volume from 89–95% (Racicot et al. 2016), further indicating that the vestibular complex of CCNHM 1000 is proportionally larger, at least by volume, than in crown odontocetes. The canaliculus cochleae for the membranous perilymphatic duct and fenestra cochleae are both short and broad, whereas these are often longer and thinner in later-diverging (especially extant) odontocetes (Racicot et al. 2016, Racicot et al. 2018). The aqueductus vestibuli is a small, short irregular cone that terminates at its aperture. Like other described cetaceans, the canal leading to the cone-shaped aqueductus vestibuli is extremely thin. The canaliculus cochleae and fenestra cochleae are both short and broad while often these are longer and thinner in other odontocetes (Racicot et al. 2016, Racicot et al. 2018).

Superficial lumps and divots on the surface of the basal whorl are associated with taphonomic artefacts such as shards of pyrite or other brightly coloured crystal going through the specimen, or the coming together of some of these remineralized areas. In some cases it is not entirely clear whether divots on the surface of the endocast are related to these veins of more dense material. In particular, a flattening of the basal whorl at the first half turn may be an anatomical feature rather than a taphonomic artefact. Otherwise, the divots are associated more

with indentations of bone and, while unusual, nonetheless reflect our best approximation of actual bony labyrinth space.

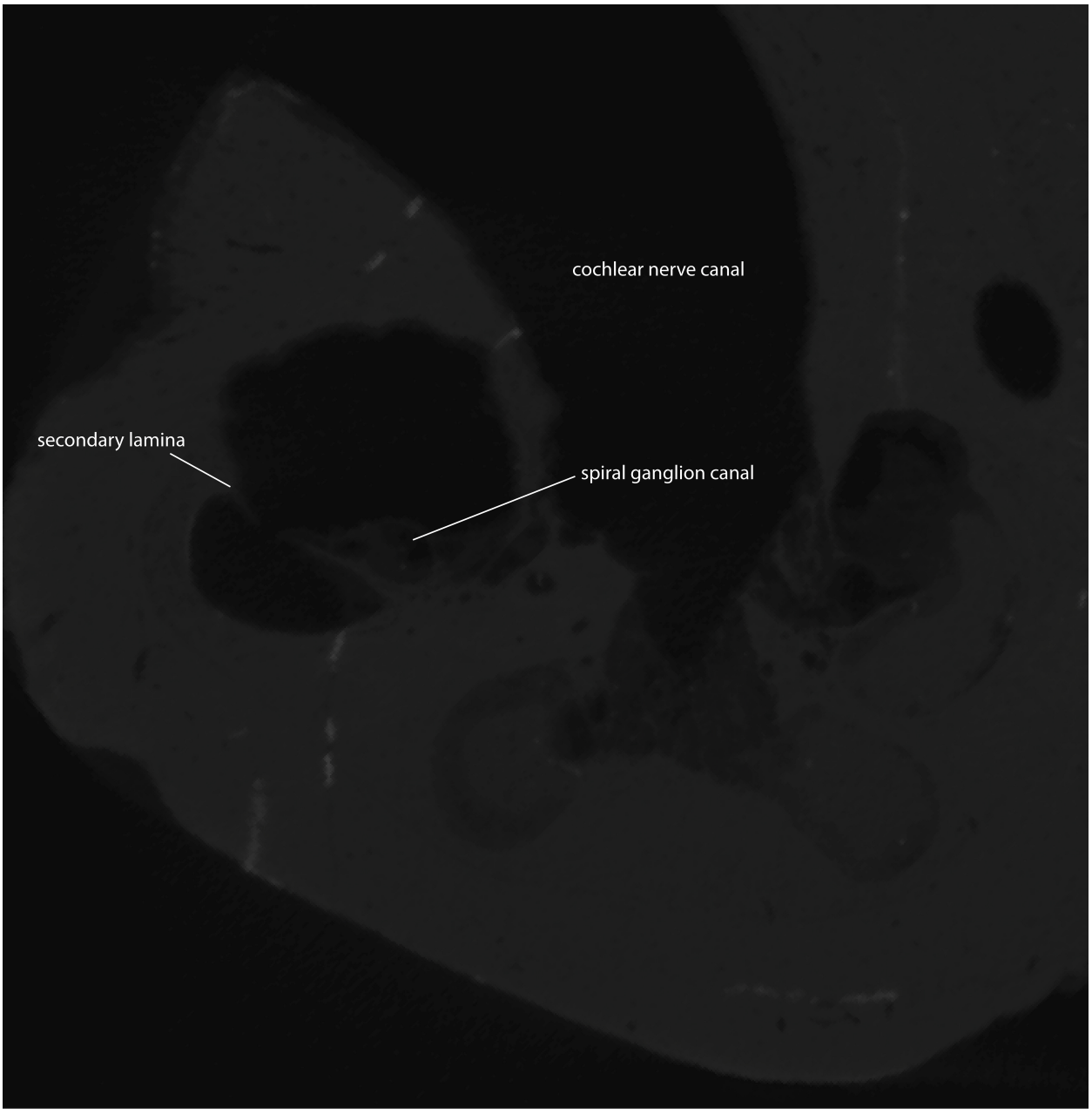

Figure S15. Labeled CT slice through the first quarter turn of the cochlea. Upper left section of the bony labyrinth is the section where the spiral ganglion canal measurements are taken.

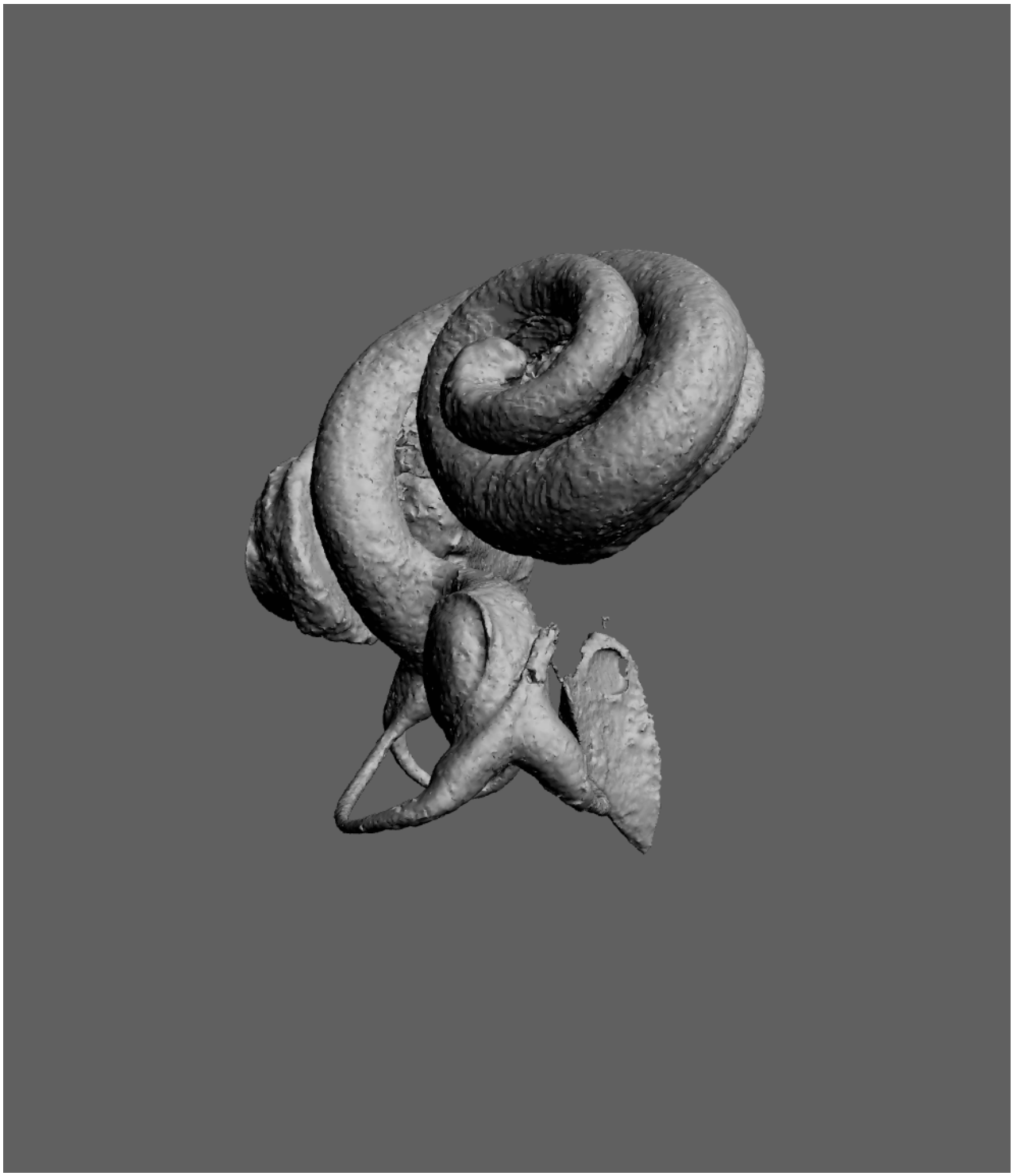

Figure S16. Three-dimensional model of the digital endocast of the bony labyrinth of CCNHM 1000.

SUPPLEMENTAL REFERENCES

Barnes and Goedert, 2001. Stratigraphy and paleoecology of Oligocene and Miocene desmostylian occurrences in Western Washington state, USA. *Bulletin of the Ashoro Museum of Paleontology* 2: 7–22.

Barnes, L. G., Kimura, M., Furusawa, H., Sawamura, H., 1995. Classification and distribution of Oligocene Aetiocetidae (Mammalia; Cetacea; Mysticeti) from western North America and Japan. *The Island Arc* 3: 392-431.

Berlin, J.C., Kirk, E.C., Rowe, T.B., 2013. Functional implications of ubiquitous semicircular canal non-orthogonality in mammals. *PLoS ONE* 8, e79585.

Berta, A., Ekdale, E.G., and Cranford, T.W. 2014. Review of the cetacean nose: Form, function, and evolution. *The Anatomical Record* 297: 2205–2215.

Boessenecker, R.W. and Fordyce, R.E., 2015. Anatomy, feeding ecology, and ontogeny of a transitional baleen whale: a new genus and species of Eomysticetidae (Mammalia: Cetacea) from the Oligocene of New Zealand. *PeerJ* 3:e1129.

Boessenecker, R.W., Fraser, D., Churchill, M., Geisler, J.H., 2017. A toothless dwarf dolphin (Odontoceti: Xenorophidae) points to explosive feeding diversification of modern whales (Neoceti). *Proceedings of the Royal Society B* 284, 20170531.

Boessenecker, R.W., Ahmed, E., Geisler, J.H., 2017. New records of the dolphin *Albertocetus meffordorum* (Odontoceti: Xenorophidae) from the lower Oligocene of South Carolina: Encephalization, sensory anatomy, postcranial morphology, and ontogeny of early odontocetes. *PLoS One* 12, e0186476.

Churchill, M., Martinez-Caceres, M., de Muizon, C., Mnieckowski, J., Geisler, J.H., 2016. The origin of high-frequency hearing in whales. *Current Biology* 26, 1–6.

Costeur, L., Grohe, C., Aguirre-Fernandez, G., Ekdale, E., Schulz, G., Muller, B., Mennecart, B. 2018. The bony labyrinth of toothed whales reflects both phylogeny and habitat preferences. *Scientific Reports* 8, 7841.

Cranford, T.W., Amundin, M., and Norris, K.S. 1996. Functional morphology and homology in the odontocete nasal complex: Implications for sound generation. *Journal of Morphology* 228: 223–285.

Cranford, T.W., McKenna, M.F., Soldevilla, M.S., Wiggins, S.M., Goldbogen, J.A., Shadwick, R.E., Krysl, P., St. Leger, J.A., Hildebrand, J.A. 2008. Anatomic geometry of sound

transmission and reception in Cuvier's Beaked Whale (*Ziphius cavirostris*). *The Anatomical Record* 291: 353–378.

Cranford, T.W., Krysl, P., and Amundin, M. 2010. A new acoustic portal into the odontocete ear and vibrational analysis of the tympanoperiotic complex. *PLoS ONE* 5, e11927.

Domning, D.P., Ray, C.E., and McKenna, M.C., 1986. Two new Oligocene desmostylians and a discussion of tethytherian systematics. *Smithsonian Contributions to Paleobiology* 59: 1–56.

Dyke, G. J., Wong, X., and Habib, M. B. 2011. Fossil plotopterid seabirds from the Eo-Oligocene of the Olympic Peninsula (Washington State, USA): Descriptions and functional morphology. *PLoS One* **6**: e25672.

Ekdale, E.G, Racicot, R.A., 2015. Anatomical evidence for low frequency sensitivity in an archaeocete whale: comparison of the inner ear of *Zygorhiza kochii* with that of crown Mysticeti. *Journal of Anatomy* 226, 22–39.

Ekdale, E.G. and Rowe, T.B. 2011. Morphology and variation within the bony labyrinth of zhelestids (Mammalia, Eutheria) and other therian mammals. *Journal of Vertebrate Paleontology* 31, 658–675.

Ekdale, E.G., 2016. Morphological variation among the inner ears of extinct and extant baleen whales (Cetacea: Mysticeti). *Journal of Morphology* 277, 1599-1615.

Fordyce, R.E., 2002. *Simocetus rayi* (Odontoceti, Simocetidae, new family); a bizarre new archaic Oligocene dolphin from the eastern North Pacific. *Smithsonian Contributions in Paleobiology* 93: 185–222.

Galatius, A., Tange Olsen, M., Steeman, M., Racicot, R.A., Bradshaw, C.D., and Miller, L.A. 2018. Raising your voice: Evolution of narrow band high frequency signals in odontocetes. *Biological Journal of the Linnean Society.* Available in Early View.

Gatesy, J., J. H. Geisler, J. Chang, C. Buell, A. Berta, R. Meredith, M. S., Springer, and M. R. McGowen. 2013. A phylogenetic blueprint for a modern whale. *Molecular Phylogenetics and Evolution* 66, 479–506.

Geisler, J.H., Luo, Z. 1996. The petrosal and inner ear of *Herpetocetus* sp. (Mammalia: Cetacea) and their implications for the phylogeny and hearing of archaic mysticetes. *Journal of Paleontology* 70, 1045–1066.

Geisler, J.H., Colbert, M.W., Carew, J.L., 2014. A new fossil species supports an early origin for toothed whale echolocation. *Nature* 508, 383–386.

Goedert, J.L. and Squires, R.L.,1993. First Oligocene records of *Calyptogena* (Bivalvia: Vesicomyidae). *The Veliger* 36: 72–77.

Goloboff, P.A., Farris, J.S., Nixon, K.C., 2008. TNT, a free program for phylogenetic analysis. *Cladistics* 24, 774-786.

Huggenberger, S., Rauschmann, M.A., Oelschläger, H.H.A. 2008. Functional morphology of the hyolaryngeal complex of the harbor porpoise (*Phocoena phocoena*): implications for its role in sound production and respiration. *The Anatomical Record* 291, 1262–1270.

Huggenberger, S., Rauschmann, M.A., Vogl, T.J., Oelschläger, H.H.A. 2009. Functional morphology of the nasal complex in the harbor porpoise (*Phocoena phocoena* L.). *The Anatomical Record* 292, 902–920.

Josse, J. and Husson, F., 2016. missMDA: A package for handling missing values in multivariate data analysis. *Journal of Statistical Software* 70, 1–31.

Ketten, D.R. 1992. The cetacean ear: Form, frequency, and evolution. In: *Marine Mammal Sensory Systems*, Edited by J. Thomas et al., Plenum Press, NY pp. 53–75.

Le, S., Josse, J, Husson, F., 2008. FactoMineR: An R package for multivariate analysis. *Journal of Statistical Software* 25, 1–18.

Liu, Z., Qi, F-Y, Zhou, Z., Ren, H-Q, Shi, P., 2014. Parallel Sites Implicate Functional Convergence of the Hearing Gene *Prestin* among Echolocating Mammals. *Molecular Biology* 31, 2415-2424.

Malinzak, M.D., Kay, R.F., Hullar, T.E., 2012. Locomotor head movements and semicircular canal morphology in primates. *Proceedings of the National Academy of Sciences* USA 109, 17814–17919.

Marx, F.G., Tsai, C-H., Fordyce, R.E. , 2015. A new early Oligocene toothed “baleen” whale (Mysticeti: Aetiocetidae) from western North America: one of the oldest and the smallest. *Royal Society open science*, 2: 150476.

McKenna, M.C., Cranford, T.W., Berta, A., Pyenson, N. 2012. Morphology of the odontocete melon and its implications for acoustic function. Marine Mammal Science 28, 690–713.

Mead, J.G. 1975. Anatomy of the external nasal passage and facial complex in the Delphinoidea (Mammalia: Cetaecea). *Smithosonian Contributions in Zoology* 207, 1–72.

Mooney, T.A., Yamato, M., Branstetter, B.K. 2012. Hearing in cetaceans: from natural history to experimental biology. *Advances in Marine Biology* 63, 197–246.

Mourlam, M.J., Orliac, M.J., 2017. Infrasonic and ultrasonic hearing evolved after the emergence of modern whales. *Current Biology* 27, 1776–1781.

Numella, S., Thewissen, J.G.M., Bajpai, S., Hussain, T., Kumar, K. Sound transmission in archaic and modern whales: Anatomical adaptations for underwater hearing. *The Anatomical Record* 290, 716–733.

Olson, S.L., 1980. A new genus of penguin-like pelecaniform bird from the Oligocene of Washington (Pelecaniformes: Plotopteridae). *Natural History Museum of Los Angeles County Contributions in Science*, 330: 51-57.

Park, T., Fitzgerald, E. M. G. and Evans, A. R., 2016. Ultrasonic hearing and echolocation in the earliest toothed whales. *Biology Letters* 12: 20160060.

Peredo, C.M. and Uhen, M.D., 2016. A new basal chaeomysticete (Mammalia: Cetacea) from the late Oligocene Pysht Formation of Washington, USA. *Papers in Palaeontology* 2: 533–554.

Peredo, C.M., Pyenson, N.D., and Uhen, M.D., 2018. Tooth loss precedes the origin of baleen in whales. *Current Biology* 28: 3992–4000.

Prothero, D.R. (ed.) 2001. Magnetic Stratigraphy of the Pacific Coast Cenozoic. Pacific Section SEPM Special Publication 91, 394 p.

Racicot, R.A., Gearty, W., Kohno, N., Flynn, J.J. 2016. Comparative anatomy of the bony labyrinth of extant and extinct porpoises (Cetacea: Phocoenidae). *Biological Journal of the Linnaean Society* 119, 831–846.

Racicot, R.A., Darroch, S.A.F., Kohno, N., 2018. Neuroanatomy and inner ear labyrinths of the narwhal, *Monodon monoceros*, and beluga, *Delphinapterus leucas* (Cetacea: Monodontidae). *Journal of Anatomy* 233, 421-439.

Reidenberg, J.S., Laitman, J. 1987. Position of the larynx in odontoceti (toothed whales). *The Anatomical Record,* 281, 98–106.

Sanders, A.E., and Geisler, J.H., 2015. A new basal odontocete from the upper Rupelian of South Carolina, U.S.A., with contributions to the systematics of *Xenorophus* and *Mirocetus* (Mammalia, Cetacea). *Journal of Vertebrate Paleontology* 35, e890107.

Velez-Juarbe, J., 2017. A new stem odontocete from the late Oligocene Pysht Formation in Washington State, USA. *Journal of Vertebrate Paleontology* 37, e1366916.

Welton, B.J. and Goedert, J.L., 2016. New fossil species of *Somniosus* and *Rhinoscymnus* (Squaliformes: Somniosidae), deep water sharks from Oligocene rocks of Western Washington State, USA. *New Mexico Museum of Natural History and Science Bulletin* 74: 309–326.